Longitudinal Modes of Elastic Waves in Isotropic Cylinders and Slabs

By A. N. HOLDEN

The general properties of the longitudinal modes in cylinders and slabs are developed with the aid of the close formal analogy between the dispersion equations for the two cases.

1. Introduction

THE classical exact treatments of the modes of propagation of elastic waves in isotropic media having stress-free surfaces but extending indefinitely in at least one dimension are those of Rayleigh[1] for semi-infinite media bounded by one plane, of Lamb[2] for slabs bounded by two parallel planes, and of Pochhammer[3] for solid cylinders. Rayleigh showed that a wave could be propagated without attenuation parallel to the surface, in which the displacement amplitude of the medium decreased exponentially with distance from the surface, at a velocity independent of frequency and somewhat lower than that of either the plane longitudinal or plane transverse waves in the infinite medium. Such "Rayleigh surface waves" have received application in earthquake theory.

For slabs or cylinders the treatments lead to a transcendental secular equation, establishing a relation (the "geometrical dispersion") between the frequency and the phase velocity, which for some time received only asymptotic application in justifying simpler approximate treatments. The past decade, however, has seen a revival of interest in the exact results[4, 5] stimulated by experimental application of ultrasonic techniques to rods[6, 9] and slabs,[7] by the use of rods and the like as acoustic transmission media, and perhaps by curiosity as to what qualitative correspondence may exist between such waves and the more intensively studied electromagnetic waves in wave guides. That this correspondence might not be close could be anticipated by observing that an attempt to build up modes by the superposition of plane waves in the medium reflected from boundaries would encounter an essential difference between the two cases: the elastic medium supports plane waves of two types (longitudinal and transverse) with different velocities, and reflection from a boundary transforms a wave of either type into a mixture of both.

On grounds both formal and physical it may be expected that solutions to the equations of small motion of the medium with a stress-free cylindrical boundary can be found with any integral number of diametral nodes of the

component of displacement along the rod, as well as for the "torsional" modes in which there is no displacement along the rod whatever. The classical results are for no such nodes, the "longitudinal" (or "elongational") modes, and for one such node, the "flexural" modes. The secular equation for modes with any number of such nodes has been exhibited by Hudson.[5] For any one of these types of mode, it may be expected that the secular equation will define a many-branched relation* between frequency and phase velocity, and that a different number of interior cylindrical nodal surfaces for the displacement components might be associated with each branch. Apart from the relatively simple torsional modes, the only branches whose properties have been intensively studied are the lowest branch of the longitudinal[4] and the lowest of the flexural[5] modes, because they (and the lowest torsional branch) are the only ones extending to zero frequency, the others exhibiting "cut-off" frequencies at which their phase velocities become infinite and below which they are rapidly attenuated as they progress through the medium.

Three qualitative results of these studies are of especial interest. In the first place, with increasing frequency the phase velocity in the lowest longitudinal and flexural branches approaches the velocity of the Rayleigh surface wave, and the disturbance becomes increasingly confined to the surface of the cylinder. In the second place, the dispersion is not monotonic as it is in the electromagnetic case: the phase velocity exhibits a minimum in the lowest longitudinal branch[4] and a maximum in the lowest flexural branch[5] with varying frequency. Finally, in the lowest longitudinal branch at least, the cylindrical nodes of the displacement components vary not only in radius but even in number with the frequency.[4]

The last result suggests that it would be difficult in practice to drive a cylindrical rod in that pure mode represented by its lowest longitudinal branch over any extended frequency range, since it is difficult to visualize a driving mechanism having suitable nodal properties. Longitudinal drivers which can be readily constructed may be expected to deliver energy to all longitudinal branches, in proportions varying with frequency. How satisfactory such a transmission device could be would depend importantly on how much the phase velocities at any one frequency differed from branch to branch.

This paper sketches the behavior of the higher longitudinal branches. That behavior could, of course, be determined exactly; Hudson[5] has shown how the calculation of the roots of the secular equations can be facilitated,

* This is true in particular of the flexural type of mode, and in his otherwise excellent treatment of flexure Hudson's statement to the contrary must be disregarded. Recent writings in this field have tended to distinguish as "branches" what in allied problems are commonly called "modes".

and Hueter[9] has used graphical methods. The alternative adopted here is a semi-quantitative treatment, assisted by extensive reference to the behavior of longitudinal waves in slabs,* for which the secular equation is simpler and closely analogous. The analogy in the case of flexural modes is considerably less close and will not be discussed.

The general consequences of the inquiry are that the higher longitudinal branches have phase velocities which are not necessarily monotonic functions of frequency. With increasing frequency, however, those velocities all approach that of the plane transverse wave,** not that of the Rayleigh surface wave (nor that of the plane longitudinal wave, as some investigators had guessed), a fact reflected perhaps in the experimental observation that driving a rod transversely usually provides purer transmission than driving it longitudinally.† Variation of nodal cylinders in location and number with frequency persists in the higher branches.

2. The Slab

The slab extends to infinity in the y, z plane and has a thickness $2a$ in the x-direction. The displacements of its parts in the x, y, z directions are u, v, w. Its material has density ρ and Lamé elastic constants λ and μ, so that its longitudinal wave velocity is $\sqrt{(2\mu+\lambda)/\rho}$ and its transverse wave velocity is $\sqrt{\mu/\rho}$. That μ should be positive is a stability requirement of energetics; λ will also be taken as positive since no material with negative λ is known.

The equations of small motion are, in vector form,

$$(2\mu + \lambda)\ \text{grad div}\ (u, v, w) - \mu\ \text{curl curl}\ (u, v, w) = \rho \frac{\partial^2}{\partial t^2}(u, v, w).$$

Solutions representing longitudinal waves propagated in the z direction can be of the form

$$u = Ue^{i(\omega t+\gamma z)}, \qquad v = 0, \qquad w = We^{i(\omega t+\gamma z)},$$

where U is an odd function, and W an even function, of x alone, ω is the frequency in radians per second, and $\gamma = \omega/c$ where c is the phase velocity. Solutions independent of y are chosen here because they provide the simplest analogues to the case of the cylinder. Substitution shows that $U = Ae^{ikx}$,

* I am indebted to Dr. W. Shockley for the suggestion that this behavior might display a close enough analogy to that of the cylinder to provide insight; the work of Morse bears out the analogy.

** The fact is noted by Bancroft.

† Private communication from H. J. McSkimin.

$W = Be^{ikz}$, is a solution (where A and B are constants measuring the amplitude), if either

$$\text{(i)}\quad k_1^2 = \frac{\rho\omega^2}{2\mu + \lambda} - \gamma^2 \quad \text{and} \quad \gamma A_1 = k_1 B_1,$$

or

$$\text{(ii)}\quad k_2^2 = \frac{\rho\omega^2}{\mu} - \gamma^2 \quad \text{and} \quad k_2 A_2 = -\gamma B_2.$$

When solutions of both types are so superposed as to make U odd and W even

$$U = iA_1 \sin k_1 x + iA_2 \sin k_2 x, \tag{1}$$

$$W = A_1 \frac{\gamma}{k_1} \cos k_1 x - A_2 \frac{k_2}{\gamma} \cos k_2 x. \tag{2}$$

The normal and tangential stresses on planes perpendicular to x are

$$X_x = (2\mu + \lambda)\frac{\partial u}{\partial x} + \lambda\left(\frac{\partial v}{\partial y} + \frac{\partial w}{\partial z}\right), \qquad X_y = \mu\left(\frac{\partial v}{\partial x} + \frac{\partial u}{\partial y}\right),$$

$$X_z = \mu\left(\frac{\partial u}{\partial z} + \frac{\partial w}{\partial x}\right)$$

and the requirement that they vanish at $x = \pm a$ leads to the boundary conditions

$$A_1(\lambda\gamma^2 + (2\mu + \lambda)k_1^2)\cos k_1 a + 2A_2\mu k_1 k_2 \cos k_2 a = 0,$$

$$2A_1\gamma^2 \sin k_1 a + A_2(\gamma^2 - k_2^2)\sin k_2 a = 0,$$

the vanishing of whose eliminant with regard to A_1 and A_2 is the secular equation. Although in principle that equation establishes a relation between γ and ω, it is more conveniently examined when expressed in terms of $\alpha \equiv k_1 a$ and $\beta \equiv k_2 a$, which are quadratically related to ω and γ by (i) and (ii). In those terms it becomes

$$\begin{aligned}(\lambda\beta^2 + (2\mu + \lambda)\alpha^2)^2 \cos\alpha \sin\beta \\ + 4(\mu + \lambda)\alpha\beta(\mu\beta^2 - (2\mu + \lambda)\alpha^2)\sin\alpha\cos\beta = 0.\end{aligned} \tag{3}$$

The physically interesting quantities can be expressed in terms of α and β, with the aid of (i) and (ii). Thus

$$\rho\omega^2 = \frac{\mu(2\mu + \lambda)}{a^2(\mu + \lambda)}(\beta^2 - \alpha^2), \quad \text{and} \tag{4}$$

$$\gamma^2 = \frac{\mu\beta^2 - (2\mu + \lambda)\alpha^2}{a^2(\mu + \lambda)}. \tag{5}$$

Hence, denoting $l \equiv \beta/\alpha$, the phase velocity $c \equiv \omega/\gamma$ is given by

$$\rho c^2 = \frac{\mu(2\mu + \lambda)(l^2 - 1)}{\mu l^2 - (2\mu + \lambda)} \equiv E, \tag{6}$$

where E is an "effective stiffness", a function of the elastic constants and l.

Since $\beta = 0$ is a trivial root of equation (3), it can be divided by β, and the expression on the left then becomes even in both α and β and (3) can be regarded as an equation in α^2 and β^2. From (4) and (5) it is evident that, if ω and γ are both to be real, α^2 and β^2 must be real and must obey the inequalities

$$\beta^2 > \alpha^2, \qquad \mu\beta^2 > (2\mu + \lambda)\alpha^2, \tag{7}$$

and thus the root $\beta = \alpha$ can be neglected. The general character of the desired roots can consequently be exhibited on a plot of β^2 against α^2. Evidently on that plot lines of slope unity are lines of constant frequency (equation 4), and lines radiating from the origin are lines of constant velocity (equation 6). As will appear later, however, it is more convenient to use a linear rather than a quadratic plot, real α being measured to the right, imaginary α to the left, of the vertical axis, and real β upward, imaginary β downward, from the horizontal axis. Here radial lines are still lines of constant velocity, but lines of constant frequency are no longer simple.

In Fig. 2 such a plot has been sketched for the first few modes of a material obeying the Cauchy condition $\lambda = \mu$; the properties shown are restricted to those derived in the following paragraphs, and are lettered in Fig. 1 to correspond with those paragraphs.

(a) By virtue of (7), the significant portions of the roots lie above and to the left of the lines $\beta^2 = \alpha^2$, $\mu\beta^2 = (2\mu + \lambda)\alpha^2$. Setting $\mu\beta^2 = (2\mu + \lambda)\alpha^2$ in (3) reveals the cut-offs at $\sin\beta = 0$ and at $\cos\alpha = 0$: in other words at $\beta^2 = n^2\pi^2$, $\alpha^2 = \frac{\mu}{2\mu + \lambda} n^2\pi^2$, and also at $\beta^2 = \frac{2\mu + \lambda}{\mu}\left(n + \frac{1}{2}\right)^2 \pi^2$, $\alpha^2 = \left(n + \frac{1}{2}\right)^2 \pi^2$, where n is any integer.

(b) Setting $\alpha = 0$ in (3), it can be seen that the roots intersect the line $\alpha^2 = 0$ at the points $\sin\beta = 0$. By calculating the derivative of β^2 with respect to α^2, those points (at which α changes from pure real to pure imaginary) can be shown not to be multiple points, and the branches to have $\frac{d\beta}{d\alpha} = 0$ and $\frac{d(\beta^2)}{d(\alpha^2)} = -\frac{8\mu(\mu + \lambda)}{\lambda^2}$, independent of branch number and negative for

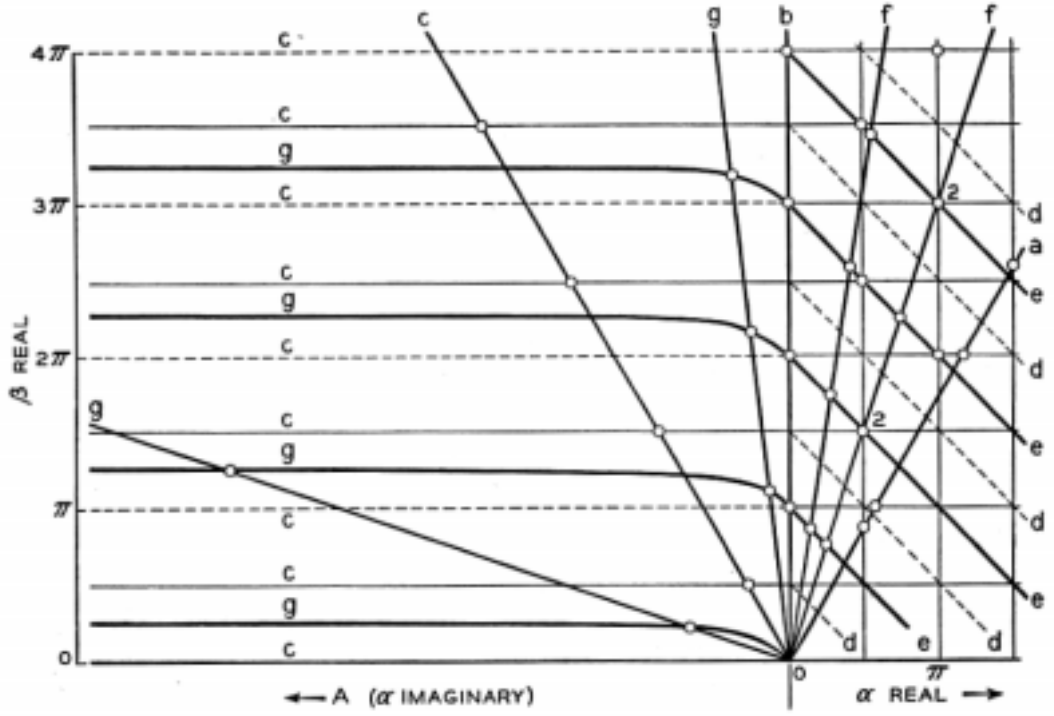

Fig. 1—Lines and intersections, discussed in the correspondingly lettered paragraphs of the text, which determine the properties of the first five branches of the longitudinal modes for a material obeying the Cauchy condition. Two coincident pairs of points are marked (2).

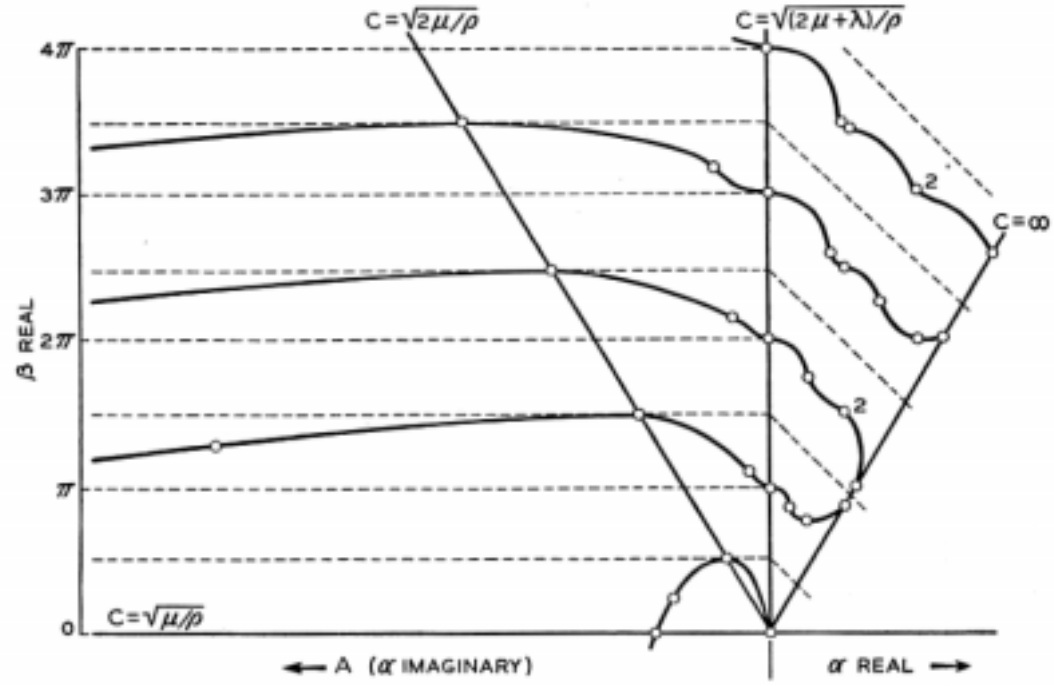

Fig. 2—A rough sketch of the branches determined by the properties illustrated in Fig. 1.

all materials. At those points the phase velocity is that of a plane longitudinal wave.

(c) Setting $\sin \beta = 0$ reduces (3) to $\alpha\beta(\mu\beta^2 - (2\mu + \lambda)\alpha^2) \sin \alpha = 0$, and hence in the region of positive β^2 and negative α^2 the roots do not intersect the horizontal lines $\beta^2 = n^2\pi^2$ $(n \neq 0)$. As can be seen from (6) this confinement implies that the velocity is asymptotic to $\sqrt{\mu/\rho}$, that of a plane transverse wave, with increasing frequency. Notice that, in the region of positive β^2 and negative α^2, β takes the values $\cos \beta = 0$ only where $\lambda\beta^2 + (2\mu + \lambda)\alpha^2 = 0$ and that the roots have zero slope there. At those points the waves have a phase velocity $\sqrt{2}$ times that of a plane transverse wave.

(d) In the region of positive β^2 and positive α^2 the roots exhibit a somewhat more complicated behavior, but confining lines can again be found: the diagonal lines $\beta = (n + \frac{1}{2})\pi - \alpha$. It is the nature of such critical lines as these which can be better exhibited on the linear than on the quadratic plot. Alternatively those lines can be written $\cos \alpha \cos \beta - \sin \alpha \sin \beta = 0$ (and thus will be shown to have analogues in the case of the cylinder), and substitution of this expression into (3) shows that if the roots intersect these lines they must do so for values of α and β satisfying the relation

$$4(\mu + \lambda)\alpha\beta(\mu\beta^2 - (2\mu + \lambda)\alpha^2) = -(\lambda\beta^2 + (2\mu + \lambda)\alpha^2)^2 \cot^2 \alpha.$$

But the inequalities (7) make such values impossible.

(e) This suggests that in that region the roots may oscillate in a somewhat irregular manner about the diagonal lines $\beta = n\pi - \alpha$. Indeed it is immediately evident that they pass through the points $\cos \beta = \cos \alpha = 0$ and $\sin \beta = \sin \alpha = 0$.

(f) Expressing those lines as $\sin \alpha \cos \beta + \cos \alpha \sin \beta = 0$, and substituting into (3), shows that additional intersections may be afforded by any roots of the quartic equation

$$(\lambda\beta^2 + (2\mu + \lambda)\alpha^2)^2 - 4(\mu + \lambda)\alpha\beta(\mu\beta^2 - (2\mu + \lambda)\alpha^2) = 0$$

which obey the inequalities (7). Discarding the root $\alpha + \beta = 0$, and dividing by α^3, yields the cubic equation

$$\lambda^2 l^3 - (2\mu + \lambda)^2 l^2 + (2\mu + \lambda)(2\mu + 3\lambda)l + (2\mu + \lambda)^2 = 0, \qquad (8)$$

whose roots are the negatives of the roots of the cubic equation for the Rayleigh surface wave velocity. It is well known that the Rayleigh cubic always yields one and only one significant positive root, and hence equation (8) can afford at most two additional significant intersections of any root of the secular equation with the line about which it oscillates. Although it

is not feasible to exhibit the roots of the Rayleigh cubic explicitly for arbitrary μ and λ, it is of some interest to exhibit its discriminant

$$D = \frac{4}{27}\lambda^4(2\mu + \lambda)^3(\mu + \lambda)^2(11\lambda^3 + 4\lambda^2\mu - 9\lambda\mu^2 - 10\mu^3),$$

and to note that for real positive values of λ and μ it changes sign only once, at approximately $\lambda/\mu = 10/9$. Hence for $\lambda/\mu > 10/9$ two roots of the Rayleigh cubic are complex, while for $\lambda/\mu < 10/9$ two roots are real and negative. For a material obeying the Cauchy condition $\lambda/\mu = 1$, the roots of the Rayleigh cubic are -3, $-3 \pm 2\sqrt{3}$; thus $l = 3, 3 + 2\sqrt{3}$, both of which obey the inequalities (7), are relevant to intersections of each branch of the roots of the secular equation with the line about which it oscillates.

(g) The results of (e) and (f) suggest the value of a similar investigation in the region of imaginary α. Here (denoting $\alpha \equiv iA$ and $L \equiv \beta/A$ where A is taken positive and real) intersections occur between the branches and the lines $\sinh A \cos \beta - \cosh A \sin \beta = 0$ when $(\lambda L^2 - (2\mu + \lambda))^2 = 4(\mu + \lambda)L(\mu L^2 + (2\mu + \lambda))$. Clearly this quartic in L has two and only two positive real roots, one greater and one less than $\sqrt{(2\mu + \lambda)/\lambda}$. In the case $\lambda = \mu$, those roots are approximately 9 and 1/3. This information, taken with that of (c), establishes that the branches are confined in the region of imaginary α to bands determined by $n\pi < \beta < (n + \frac{1}{2})\pi$, having one tangency to the lines $\beta = (n + \frac{1}{2})\pi$; and that at values of A greater than correspond to the smaller root of l, the branches lie in the bands $n\pi < \beta < (n + \frac{1}{4})\pi$.

It is convenient to obtain assurance that in general the branches do not intersect at any point by noting that the confining lines of paragraphs (c) and (d) define bands within each of which in general one and only one cut-off point falls. Pivoting a ruler about the origin of Fig. 1, and recalling the cut-off conditions, avails. Degenerate cases arise when the elastic constants satisfy a condition $2\mu + \lambda = n^2\mu$ where n is an integer; in those cases some cut-off points coincide in pairs on some confining lines. Calculation of derivatives at those points shows that the cases are not otherwise exceptional: the pair of roots forms a continuous curve which is tangent to the cut-off line at the double cut-off point.

From (6) it follows that the phase velocity will have a maximum or a minimum with frequency if $\frac{d(\beta^2)}{d(\alpha^2)} = \frac{\beta^2}{\alpha^2}$. That condition requires

$$\tan^2\alpha = -\frac{(\lambda\beta^2 + (2\mu + \lambda)\alpha^2)^2(\lambda^2\beta^2 + (2\mu + \lambda)(2\mu + 3\lambda)\alpha^2)}{4(\mu + \lambda)(2\mu + \lambda)^2\alpha^2(\beta^2 - \alpha^2)(\mu\beta^2 - (2\mu + \lambda)\alpha^2)}.$$

In the region of positive β^2 and α^2 and of the inequalities (7), this is impossible, but when α^2 is negative the condition may be satisfied. If it is satisfied in the higher branches, however, it must be satisfied an even number of times in any branch, so that the branch exhibits as many maxima as

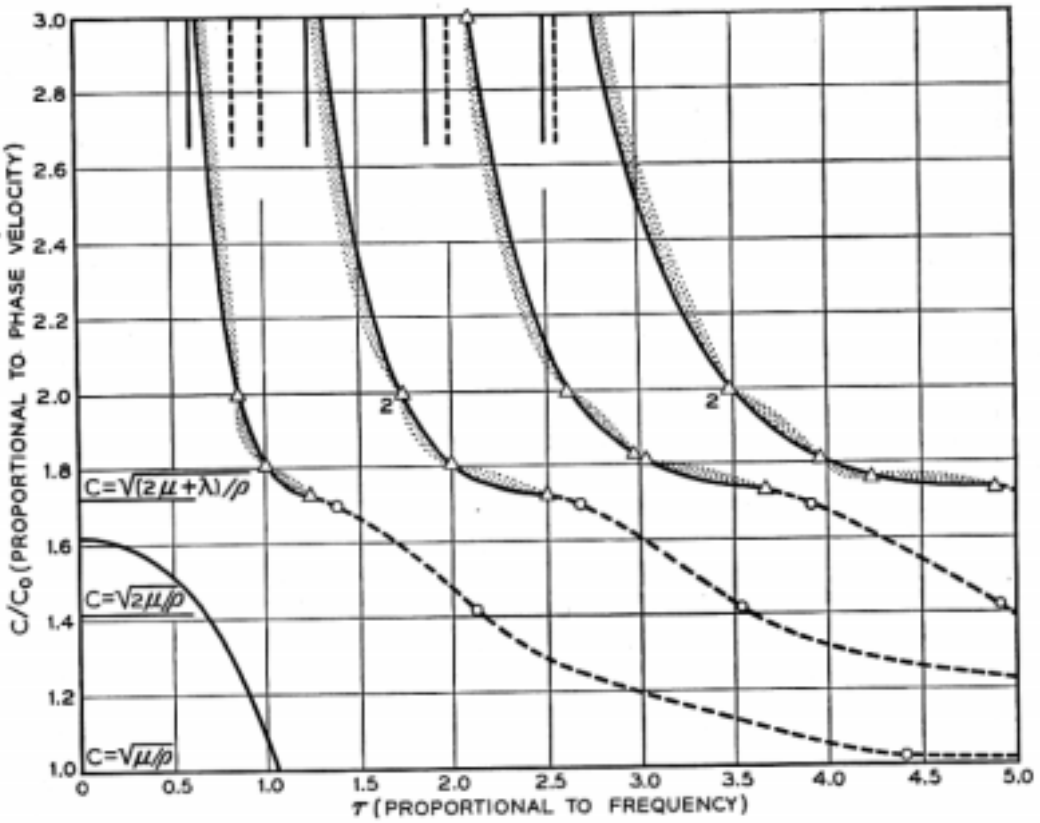

Fig. 3—The beginnings of the dispersion curves inferred from Figs. 1 and 2. The solid shaded lines are the curves about which the branches oscillate, intersecting them at the triangles and lying on the shaded side of them elsewhere, and the dashed extensions are the branches themselves. For increasing τ these branches all become asymptotic to the base line. The dashed lines at the top are the true cut-off frequencies; the solid "cut-off" lines are the asymptotes of the shaded curves. The beginning of the lowest branch is shown at the lower left; it becomes asymptotic to a line below this plot,

$$\frac{c}{c_0} = \sqrt{2 - \frac{2}{\sqrt{3}}},$$

after passing through a shallow minimum.

minima, for clearly the phase velocity is a decreasing function of frequency near the cut-off, and the velocity can also be shown to approach its asymptotic value at high frequencies from above in the higher branches.

In finally displaying the dispersion curves (Fig. 3) it is convenient to use as reduced variables τ, the number of plane transverse wave lengths in

one slab thickness (which is proportional to the frequency), and $\frac{c}{c_0}$, the ratio of the velocity to that of a plane transverse wave. Evidently

$$\tau^2 \equiv \left(\frac{\omega a}{\pi c_0}\right)^2 = \frac{1}{\pi^2} \cdot \frac{2\mu + \lambda}{\mu + \lambda} (\beta^2 - \alpha^2); \qquad \left(\frac{c}{c_0}\right)^2 = \frac{(2\mu + \lambda)(l^2 - 1)}{\mu l^2 - (2\mu + \lambda)},$$

where $c_0 \equiv \sqrt{\mu/\rho}$.

For completeness, the lowest branch will be briefly sketched: that which originates at $\alpha = \beta = 0$. A calculation of $\frac{d(\beta^2)}{d(\alpha^2)}$ at that point yields only one non-trivial root, $-(2\mu + \lambda)(2\mu + 3\lambda)/\lambda^2$, and thus the phase velocity at low frequencies is found to correspond, as would be expected, with that given by the stiffness (a semi-Young's modulus, so to speak) of a material displacement-free in the x-direction but not in the y-direction, $E = 4\mu(\mu + \lambda)/(2\mu + \lambda)$. Since lines radiating from the origin of the (β^2, α^2) plot are lines of constant velocity, the dispersion curve for this branch starts with zero slope. The root curves over, intersecting the line $\lambda\beta^2 + (2\mu + \lambda)\alpha^2 = 0$ at $\beta = \frac{\pi}{2}$, and intersects the line $\beta^2 = 0$ again at A^2 $(\alpha = iA)$ where $(2\mu + \lambda)\, A \cosh A = 4(\mu + \lambda) \sinh A$. For large negative α^2 and β^2, equation (3) approaches

$$\lambda^2 l^4 + 4\mu(\mu + \lambda)l^3 + 2\lambda(2\mu + \lambda)l^2 - 4(2\mu + \lambda)(\mu + \lambda)l + (2\mu + \lambda)^2 = 0,$$

which after discarding the trivial root $l = 1$ leaves the Rayleigh cubic. In the case of this one branch, the phase velocity approaches its asymptotic value at high frequencies from below, and hence the dispersion curve must have an odd number of maxima and minima, and in particular at least one minimum, as was discovered by numerical calculation for the corresponding branch in the case of the cylinder by Bancroft.[4]

The complicated behavior of the displacements in the higher branches is sufficiently illustrated by a brief consideration of their nodes: the values of x at which the displacement is entirely along or entirely across the slab. From (1) and the boundary conditions, the x-dependence U of the displacement component perpendicular to the slab will be given by

$$K_1 U = (\lambda\beta^2 + (2\mu + \lambda)\alpha^2) \sin\beta \sin\frac{\alpha x}{a} + 2(\mu\beta^2 - (2\mu + \lambda)\alpha^2)\sin\alpha \sin\frac{\beta x}{a} \tag{1a}$$

or by

$$K_2 U = 2(\mu + \lambda)\alpha\beta \cos\beta \sin\frac{\alpha x}{a} - (\lambda\beta^2 + (2\mu + \lambda)\alpha^2) \cos\alpha \sin\frac{\beta x}{a} \tag{1b}$$

where $K_1 = (\lambda\beta^2 + (2\mu + \lambda)\alpha^2)K \sin\beta$, $K_2 = 2(\mu + \lambda)\alpha\beta K \cos\beta$, at all points (α, β) satisfying (3). Similarly from (2) and the boundary conditions, the x-dependence W of the displacement component along the slab will be given by

$$K_3 W = (\lambda\beta^2 + (2\mu + \lambda)\alpha^2) \sin\beta \cos\frac{\alpha x}{a} - 2(\mu + \lambda)\alpha\beta \sin\alpha \cos\frac{\beta x}{a} \tag{2a}$$

or by

$$K_4 W = 2(\mu\beta^2 - (2\mu + \lambda)\alpha^2) \cos\beta \cos\frac{\alpha x}{a} + (\lambda\beta^2 + (2\mu + \lambda)\alpha^2) \cos\alpha \cos\frac{\beta x}{a}, \tag{2b}$$

$$K_3 = i\alpha\gamma a(\mu + \lambda)\frac{\lambda\beta^2 + (2\mu + \lambda)\alpha^2}{\mu\beta^2 - (2\mu + \lambda)\alpha^2} K \sin\beta, \quad K_4 = 2i\alpha\gamma a(\mu + \lambda)K \cos\beta.$$

Examine now, for example, a material for which $\lambda = \mu$, in the branch whose cut-off is at $\beta = 2\pi$, $\alpha = 2\pi/\sqrt{3}$. It can be verified at once that the nodes of the two components at some of the values of (α, β) discussed earlier are described by the following table $\left(\text{in which } t \equiv \cos\frac{\pi x}{a}\right)$:

α	β	Values of x/a for nodes of U	Values of x/a for nodes of W
$2\pi/\sqrt{3}$	2π	0, ± two values given by $2/\sqrt{3} \sin 2\pi x/a\sqrt{3} = \cos 2\pi/\sqrt{3} \sin 2\pi x/a$	$\pm\frac{1}{4}, \pm\frac{3}{4}$
π	2π	0, ± 1, ± one value given by $14t + 8 = 0$	± two values given by $14t^2 - 2t - 7 = 0$
$\pi/2$	$5\pi/2$	0, ± two values given by $22t^2 + 11t - 2 = 0$	± 1, ± one value given by $5t^2 - 15t - 11 = 0$
0	3π	0, $\pm\frac{1}{3}, \pm\frac{2}{3}, \pm 1$	no nodes
$7\pi i/2\sqrt{3}$	$7\pi/2$	0, $\pm\frac{2}{7}, \pm\frac{4}{7}, \pm\frac{6}{7}$	$\pm\frac{1}{7}, \pm\frac{3}{7}, \pm\frac{5}{7}, \pm 1$
$i\infty$	3π	0, $\pm\frac{1}{3}, \pm\frac{2}{3}, \pm 1$	$\pm\frac{1}{6}, \pm\frac{3}{6}, \pm\frac{5}{6}$

It is to be noted in general that the nodal variations become less extreme at high frequencies, since for all branches except the lowest U and W tend

to become proportional to $\sin\frac{\beta x}{a}$ and $\cos\frac{\beta x}{a}$ respectively, and β approaches the value $n\pi$ where n is the branch number in order of increasing cut-off frequency, with $n = 0$ ascribed to the lowest branch. Thus the feeling, derived from more familiar cases of wave motion, that the order in which the branches arrange themselves should be correlated with the number of nodes they display retains an asymptotic validity here, in respect of each displacement component.

Nodes of absolute displacement will occur only at special frequencies. With the notation $\alpha' \equiv \frac{\alpha x}{a}, \beta' \equiv \frac{\beta x}{a}$, the conditions for their occurrence can be written

$$(\mu\beta'^2 - (2\mu + \lambda)\alpha'^2)\sin\beta'\cos\alpha' + (\mu + \lambda)\alpha'\beta'\cos\beta'\sin\alpha' = 0,$$

$$\frac{\sin 2\alpha'}{\sin 2\alpha} = \frac{\sin 2\beta'}{\sin 2\beta}, \qquad \frac{\beta'}{\alpha'} = \frac{\beta}{\alpha}, \qquad \beta' \leq \beta, \qquad \alpha' \leq \alpha,$$

taken together with (3).

3. The Cylinder

Procedures analogous to those of the preceding section, and presented by Love[5], lead to Pochhammer's secular equation, which in the present notation* is

$$\begin{aligned}(\lambda\beta^2 + (2\mu + \lambda)\alpha^2)^2 J_0(\alpha)J_1(\beta) \\ + 4(\mu + \lambda)\alpha\beta(\mu\beta^2 - (2\mu + \lambda)\alpha^2)J_1(\alpha)J_0(\beta) \\ + 2(\mu + \lambda)(2\mu + \lambda)\alpha(\alpha^2 - \beta^2)J_1(\alpha)J_1(\beta) = 0,\end{aligned} \tag{9}$$

where (4), (5) and (6) still hold, with a signifying the radius of the rod. The analogy between (3) and the first two terms of (9) is striking. Again the roots $\beta = 0$ and $\beta = \alpha$ can be neglected, and the equation when divided by β becomes even in α and β, and a plot of β^2 against α^2 becomes appropriate, with the restrictions (7) as to regions of significance. The following paragraphs are lettered to correspond with their analogues of the preceding section.

(a) Setting $\mu\beta^2 = (2\mu + \lambda)\alpha^2$ in (9) reveals the cut-offs at $J_1(\beta) = 0$ and at $(2\mu + \lambda)\alpha J_0(\alpha) = 2\mu J_1(\alpha)$.

(b) Setting $\alpha = 0$ in (9), it can be seen that the roots intersect the line

* In comparing this treatment with that of Hudson[5], interpret his symbols

$$x \to \beta,\ y \to \alpha,\ \tau_0 \to \frac{\omega a}{c_0},\ \alpha \to \frac{2\mu}{2\mu+\lambda}.$$

$\alpha^2 = 0$ at the points $J_1(\beta) = 0$, traversing them with $\frac{d(\beta^2)}{d(\alpha^2)} = \frac{-4\mu(\mu+\lambda)}{\lambda^2}$, or half that of their analogues. Again it is only at those points that the phase velocity has the value $\sqrt{(2\mu+\lambda)/\rho}$.

(c) Setting $J_1(\beta) = 0$ reduces (9) to $\alpha\beta(\mu\beta^2 - (2\mu+\lambda)\alpha^2)J_1(\alpha) = 0$, and hence the roots are confined between the horizontal lines $J_1(\beta) = 0$ in the region of positive β^2 and negative α^2, and the velocity is asymptotic to $\sqrt{\mu/\rho}$ with increasing frequency. They meet the line $\lambda\beta^2 + (2\mu+\lambda)\alpha^2 = 0$ at the points $\beta J_0(\beta) - J_1(\beta) = 0$, or in other words at the maxima and minima of $J_1(\beta)$,* where again the phase velocity is $\sqrt{2\mu/\rho}$.

(d) In the case of the cylinder confining lines** are

$$\left[J_1'(\alpha) + \frac{\lambda(\beta^2-\alpha^2)}{\alpha(\lambda\beta^2+(2\mu+\lambda)\alpha^2)}J_1(\alpha)\right]J_1'(\beta) - J_1(\alpha)J_1(\beta) = 0,$$

since substitution shows that intersection of (9) with these lines would require

$$\frac{4(\mu+\lambda)\alpha\beta(\mu\beta^2-(2\mu+\lambda)\alpha^2)}{(\lambda\beta^2+(2\mu+\lambda)\alpha^2)^2}J_1^2(\alpha) = -\left[J_1'(\alpha) + \frac{\lambda(\beta^2-\alpha^2)}{\alpha(\lambda\beta^2+(2\mu+\lambda)\alpha^2)}J_1(\alpha)\right]^2,$$

which cannot be satisfied by permitted values of α^2 and β^2.

(e) This suggests that in that region the roots may oscillate about the lines

$$J_1(\alpha)J_1'(\beta) + J_1(\beta)\left[J_1'(\alpha) + \frac{\lambda(\beta^2-\alpha^2)}{\alpha(\lambda\beta^2+(2\mu+\lambda)\alpha^2)}J_1(\alpha)\right] = 0.$$

In fact, in view of the equivalence $J_1'(x) = J_0(x) - \frac{1}{x}J_1(x)$, those lines can be seen to have points in common with the roots of the secular equation at $J_1(\alpha) = 0$, $J_1(\beta) = 0$, and at

$$J_1'(\beta) = 0, \qquad J_1'(\alpha) + \frac{\lambda(\beta^2-\alpha^2)}{\alpha(\lambda\beta^2+(2\mu+\lambda)\alpha^2)}J_1(\alpha) = 0.$$

(f) Substituting the expression for the lines of (e) into (9) shows that again additional intersections may be afforded by suitable roots of the cubic equation (8).

* The analogy to the corresponding intersections for the slab at the maxima and minima of $\sin\beta$ is noted by Lamb, ref. 2, p. 122, footnote.

** There are infinitely many such families of lines but none carries the analogy with the slab to the point of being independent of the elastic constants. The families used in (d) and (e) serve the present purpose as simply as any.

(g) In the region $\alpha = iA$, the analogous lines are given by

$$iJ_1(iA)J_1'(\beta) + J_1(\beta)\left[J_1'(iA) - \frac{\lambda(\beta^2 + A^2)}{A(\lambda\beta^2 - (2\mu + \lambda)A^2)}\, iJ_1(iA)\right] = 0,$$

with which intersections occur for the same values of β/A as in the slab.

These results permit visualization of a counterpart to Fig. 1 for the cylindrical case. In it the critical lines radiating from the origin are the same. The horizontal lines, instead of being evenly spaced by $\pi/2$, are spaced as the zeros, maxima, and minima of $J_1(\beta)$. The vertical lines, again no longer evenly spaced, are replaced alternately by straight vertical lines $J_1(\alpha) = 0$ and by the curved "vertical" lines $J_0(\alpha) = \dfrac{2(\mu + \lambda)\alpha}{\lambda\beta^2 + (2\mu + \lambda)\alpha^2} J_1(\alpha)$ which lie between their straight companions and approach $J_0(\alpha) = 0$ as β becomes large. Finally the confining lines, and the lines about which the branches oscillate, become the curves defined in (d) and (e), which can be seen to follow a course not dissimilar to the diagonal course of their predecessors, passing through the intersections of the new horizontals and verticals.

Again the branches do not intersect, except for pair-wise coincidence of cut-offs on one or another of the lines (d) when the elastic constants obey special relations. Thus the dispersion curves to which Hudson[5] assigns certain of Shear and Focke's data cannot be taken (and indeed Hudson does not suggest that they must be taken) as corresponding to higher branches of the longitudinal modes, since the former curves intersect one another, and the latter cannot unless anisotropy modifies their behavior qualitatively. The assignments could represent modes other than longitudinal. The more recent results of Hueter[9] show essentially the behavior of Fig. 3.

In view of the closeness of the analogy thus revealed, it may be taken as probable that qualitative correspondence will obtain quite generally between the longitudinal modes of the slab and those of the cylinder.

References

1. Lord Rayleigh, *Proc. Lond. Math. Soc. 17*, 4 (1885).
2. H. Lamb, *Proc. Roy. Soc. Lond. A, 93*, 114 (1917).
3. L. Pochhammer, *J. reine angew. Math.* (Crelle) *81*, 33 (1875).
4. D. Bancroft, *Phys. Rev. 59*, 588 (1941).
5. G. E. Hudson, *Phys. Rev. 63*, 46 (1943).
6. S. K. Shear and A. B. Focke, *Phys. Rev. 57*, 532 (1940).
7. R. W. Morse, *Jl. Acous. Soc. Am. 20*, 833 (1948).
8. A. E. H. Love, "Mathematical Theory of Elasticity," Cambridge 1927, 4th Ed., p. 287.
9. T. F. Hueter, *Jl. Acous. Soc. Am. 22*, 514 (1950); *Zeit. angew. Phys. 1*, 274 (1949).

Frequency Dependence of Elastic Constants and Losses in Nickel

By R. M. BOZORTH, W. P. MASON and H. J. McSKIMIN

The elastic constants of nickel crystals, and their variation with magnetic field (ΔE effect), have been measured by a 10-megacycle ultrasonic pulsing method. The constants of three crystals agree well with one another when the crystals are magnetically saturated, but vary with domain distribution when demagnetized. The maximum ΔE effect observed is much less (3%) than has been observed at lower frequencies (20%). By measuring the ΔE effect and the decrement of polycrystalline rods at low frequencies, it is shown that the small effect observed at 10 megacycles is due to a relaxation in the domain wall motion due to micro-eddy-current damping.

From the initial slope of the decrement-frequency curve, and also from the frequency of maximum decrement, the size of the average domain is found to be about 0.04 mm. Actual domains in single nickel crystals have been observed optically by Williams, who finds domain widths of 0.02 to 0.2 mm.

THE three elastic constants of nickel have been determined in several single crystals by measuring the velocity of pulses of elastic waves of frequency 10 mc/s and duration 0.001 sec. The method has been described by McSkimin[1] and the preliminary results on nickel have already been reported briefly.[2]

It is well known that Young's modulus, E, increases with magnetization, and changes in E (the "ΔE effect") by 15 to 30 per cent have been observed at room temperature and changes by greater amounts at higher temperatures.[3] It was surprising to find then, in our own experiments at 10 mc, that the greatest change was only about 3 per cent. It then occurred to us that, at such a high frequency, relaxation of the domain wall motion by micro-eddy-current damping might be expected. This led to the investigation of the frequency dependence of ΔE and of the logarithmic decrement, δ, in polycrystalline nickel, and the results obtained support the theory and give information about domain size, as described below. Calculations[4] based on the equations of domain wall motion give results which agree with the experiments.

A number of experiments[3] have already established the existence of micro-eddy-current losses in magnetic materials subjected to elastic vibrations. These losses have their origin in the local stress-induced changes of magnetization of the domains of which magnetic materials are composed. The change in magnetization of one domain will give rise to eddy-currents around it and in it, and the consequent loss in energy depends on the frequency f and the resistivity R, and on the size and shape of the region in which the change in magnetization occurs. These losses are in addition to the *macro-*

eddy-current losses, due to the relatively uniform changes in magnetization of a magnetized specimen that occur during a change in stress.

Calculations of the logarithmic decrement, δ_i, attributable to micro-eddy-currents, have been made by Becker and Döring[3] and by one of the writers.[4] According to these calculations when the material is composed of plate-like domains of thickness l, in which magnetization changes by boundary displacement, the decrement for nickel, which has its directions of easy magnetization parallel to [111] directions, is given by the relation

$$\delta = \frac{\mu_0 E_s \lambda_{111}^2}{5 I_s^2} \left[\frac{5 c_{44}}{c_{11} - c_{12} + 3 c_{44}} \right]^2 \frac{f/f_0}{1 + f^2/f_0^2} \tag{1}$$

where f_0, the relaxation frequency for domain wall motion is $f_0 = \dfrac{\pi R}{24 \mu_0 l^2}$, I_s is the saturation magnetization, E_s is the saturated value of Young's modulus, μ_0 is the initial permeability, R the electrical resistivity, λ_{111} the saturation magnetostriction along the [111] direction, and c_{11}, c_{12} and c_{44} the three elastic constants of nickel which are evaluated in this paper. For low frequencies the initial slope of the decrement vs frequency curve is

$$\frac{\delta}{f} = \frac{24 E_s \mu_0^2 l^2 \lambda_{111}^2}{5 \pi R I_s^2} \left[\frac{5 c_{44}}{c_{11} - c_{12} + 3 c_{44}} \right]^2 \tag{2}$$

As the frequency is increased the decrement rises to a maximum and then declines asymptotically to zero. Both the initial slope of the δ vs f curve and the frequency at which the maximum occurs are measures of the domain size. The initial slope has already been used to evaluate the size of the domains in 68 Permalloy.[5] It is shown in the present work that the maximum occurs in polycrystalline nickel at a frequency consistent with the dimensions of domains observed by Williams and Walker[6] in single crystals of nickel.

Elastic Constants and Damping in Single Crystals

The nickel crystals used here were grown by slow cooling of the melt in a molybdenum wound resistance furnace, by a method previously described.[7] They were cut with major surfaces parallel to (110) planes and were placed between two fused quartz rods as shown in Fig. 1. Measurements of the elastic constants were made as described in detail by McSkimin,[1] by measuring the velocity of propagation of 10 mc pulses. In order to obtain a number of reflections in the crystal, films of polystyrene approximately $\frac{1}{4}$ wavelength thick are placed between the rods and the nickel crystal. This has the effect of lowering the impedances next to the nickel to small values and hence nearly perfect reflections at the two surfaces are obtained. The frequency is varied until successive reflections occur in phase, and the velocity is then calculated from the frequency and the dimensions of the crystal.

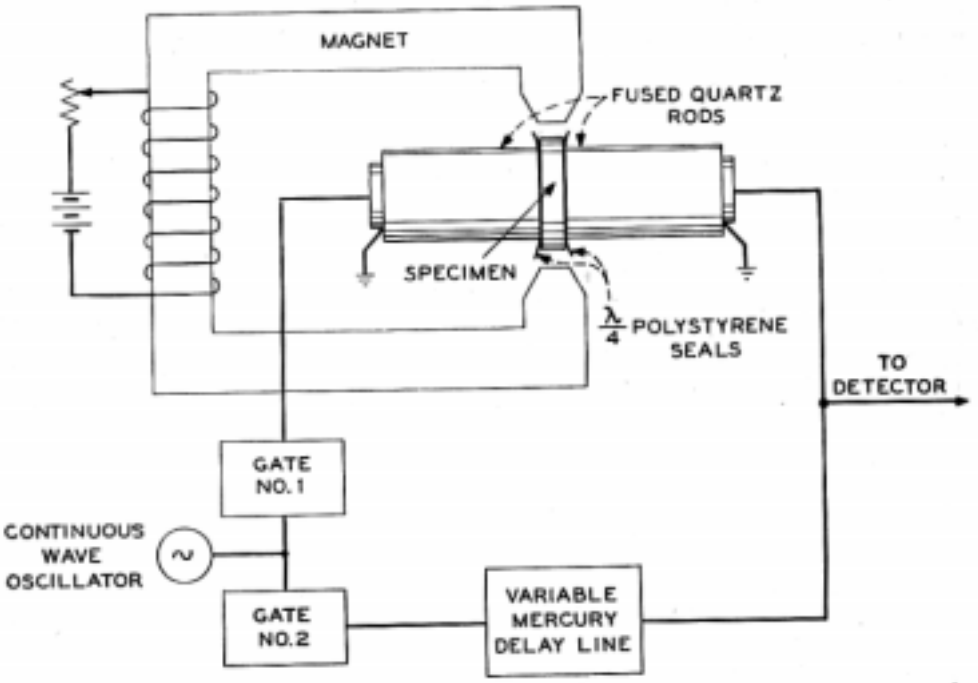

Fig. 1—Experimental arrangement for determining the elastic constants and ΔE effect in single nickel crystals.

TABLE I
ORIENTATION AND ELASTIC CONSTANTS

Direction of Propagation	Direction of Particle Motion	Type of Vibration	Equation for Velocity	Measured Velocity (cm/sec)	Elastic constants (dynes/cm²)
110	110	Longitudinal	$v = \sqrt{(c_{11} + c_{12} + 2c_{44})/2\rho}$	6.03×10^{5}*	$c_{11} + c_{12} + 2c_{44} = 6.47 \times 10^{12}$
110	$1\bar{1}0$	Shear 1	$v = \sqrt{(c_{11} - c_{12})/2\rho}$	2.26×10^{5}	$c_{11} - c_{12} = 0.90 \times 10^{12}$
110	001	Shear 2	$v = \sqrt{c_{44}/\rho}$	3.65×10^{5}	$c_{44} = 1.185 \times 10^{12}$

* A slight correction has been made for this value.

The velocities for one demagnetized crystal[1] were found to have the values shown by Table I. These values of velocity, and a density of 8.90 for the single crystal, give values for the demagnetized elastic constants of

$$c_{11} = 2.50, \qquad c_{12} = 1.60, \qquad c_{44} = 1.185 \tag{3}$$

all in 10^{12} dynes/cm².

To obtain the ΔE effect, the whole unit was placed between the jaws of a large electromagnet. Since the crystal was about 2.5 centimeters in diameter but only 0.472 cm thick, saturation could be obtained more easily along the long directions of the crystal. Figure 2 shows the changes in velocity of propagation along the [110] direction, caused by magnetization

along [001], for the shear mode with particle motion along [1$\bar{1}$0]. Fields of about 10,000 were attainable but a maximum field of about 6000 was usually used. The velocity increases by 2.6 per cent at the saturated value. On decreasing the field to zero the velocity drops below the original value

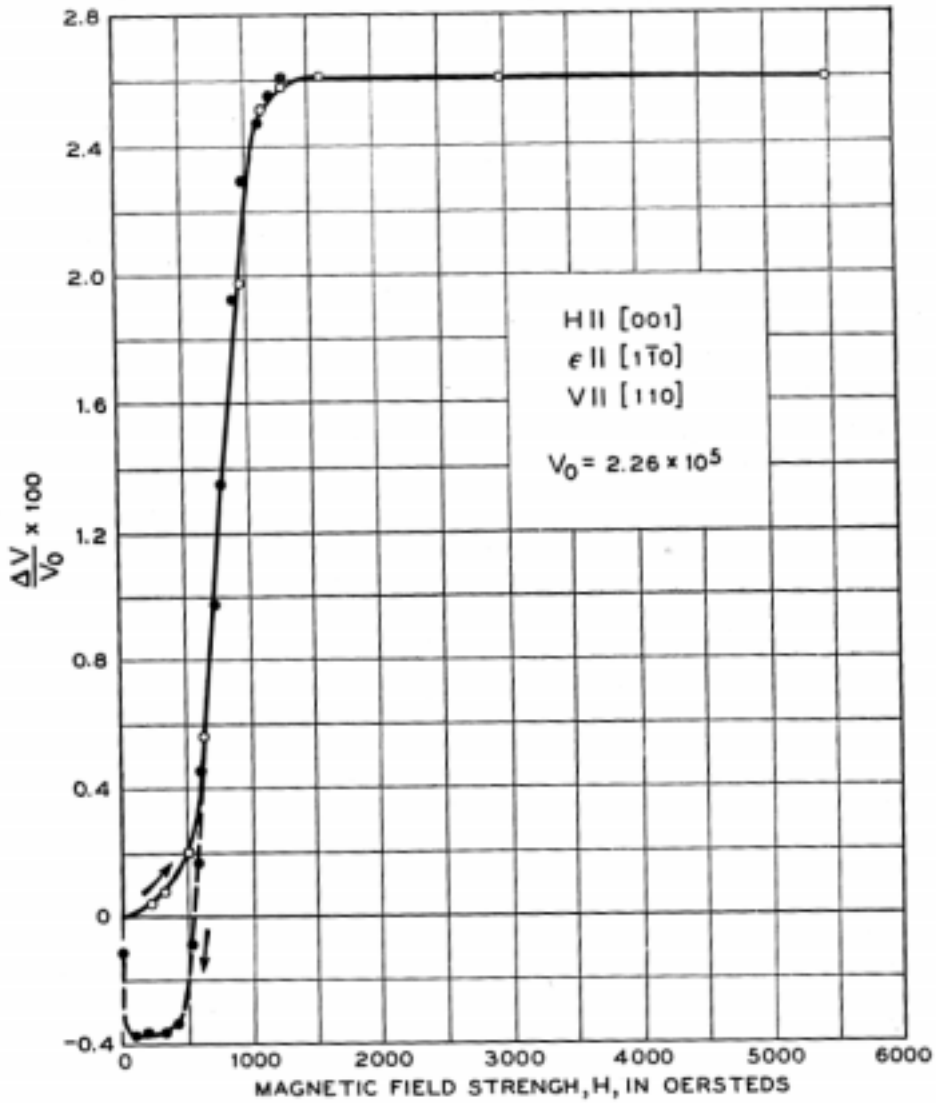

Fig. 2—Change in velocity in percent from demagnetized value as a function of the magnetizing field for a shear wave in a (110) section when the particle velocity ϵ is along the [1$\bar{1}$0] direction and the field H along the [001] direction.

for the demagnetized state, but it has practically the initial value when the crystal is again demagnetized. The lower value of velocity for the return curve indicates that the free energy is lower for some arrangement of the elementary domains other than the demagnetized state.

Figure 3 shows the attenuation in decibels per trip as a function of mag-

netization. The loss drops from about 7 db to 1 db as the crystal becomes magnetized. The low value is the remanent loss caused by the energy lost to the terminations, so that one can say that the losses due to micro-eddy-current and micro-hysteresis are 6 db per trip or 12.7 db per centimeter for this mode of motion. The Q of the crystal can be shown to be equal to

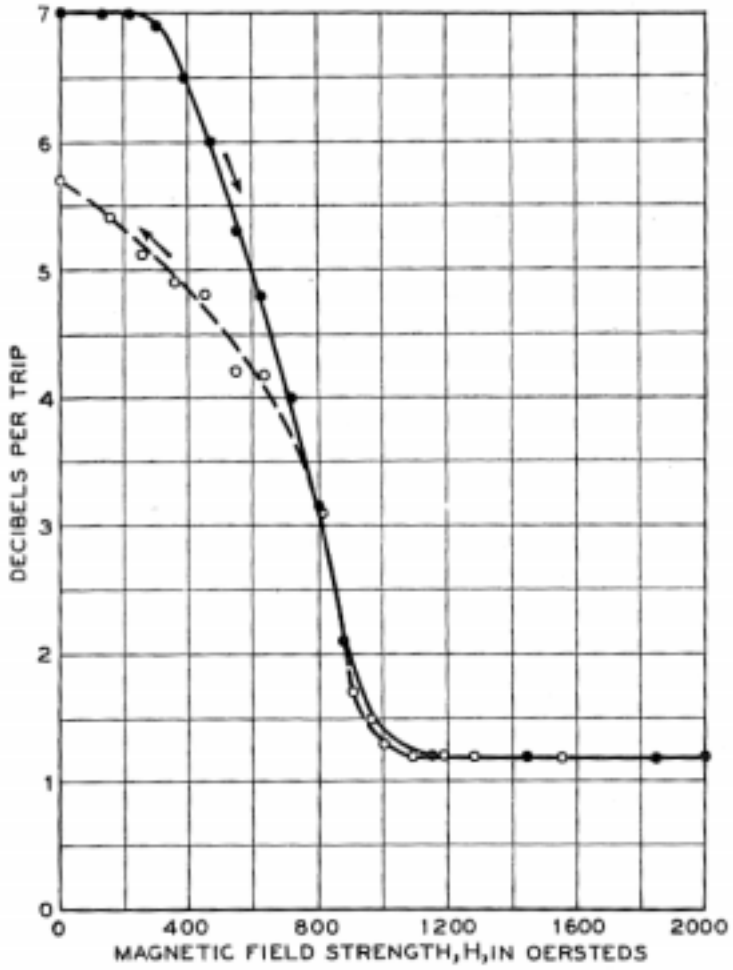

Fig. 3—Loss per trip (0.472 cm) as a function of magnetizing field for shear wave of Fig. 2.

the phase shift in radians divided by twice the attenuation in nepers per cm, or

$$Q = \frac{2\pi f/v}{2\ (db \text{ per cm})/8.68} \tag{4}$$

and our results give $Q = 94$, corresponding to a decrement of $\pi/Q = 0.033$.

Figure 4 shows a measurement of the same mode when the field is applied along the [110] direction. The velocity approaches a slightly different

limit on account of the "morphic" effect discussed in another paper.[8] If we average the two values the effective elastic constant for saturation becomes

$$c_{11}^s - c_{12}^s = 0.954 \times 10^{12} \text{ dynes/cm}^2. \quad (5)$$

Measurements for the field along the thickness did not produce saturation and are not shown.

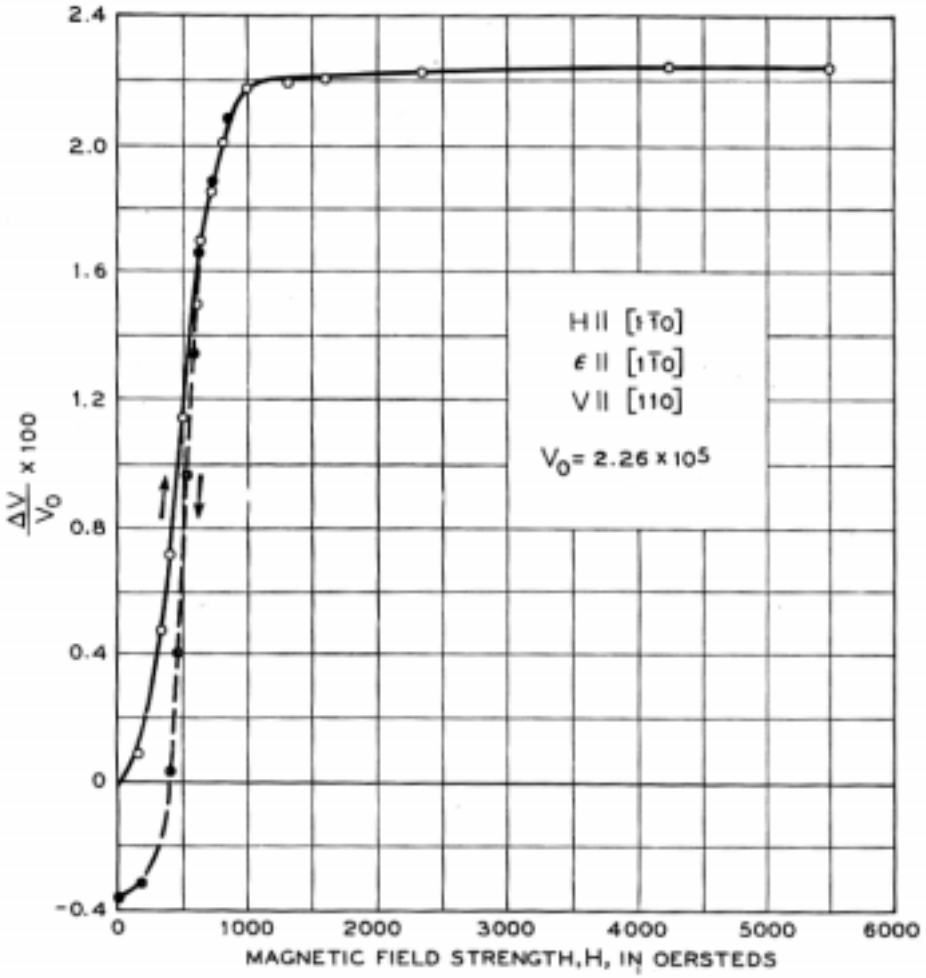

Fig. 4—Change in velocity in percent from demagnetized value as a function of the magnetizing field for a shear wave in a (110) section when the particle velocity is along the $[1\bar{1}0]$ direction and the field along the $[1\bar{1}0]$ direction.

Figures 5 and 6 show similar measurements for the other shear mode (Shear 2 of Table I) for two directions of the magnetic field. Averaging the two limiting values, the constant c_{44} at saturation becomes

$$c_{44}^s = 1.22 \times 10^{12} \text{ dynes/cm}^2 \quad (6)$$

The Q and decrement for this case become approximately 110 and 0.028.

Figures 7 and 8 show measurements for the longitudinal mode. Variations of about 0.6 per cent in the velocity are obtained, and the saturated elastic constants, Q and decrement are

$$c_{11}^s + c_{12}^s + 2c_{44}^s = 6.55 \times 10^{12}, \qquad Q = 390, \qquad \delta = 0.008 \quad (7)$$

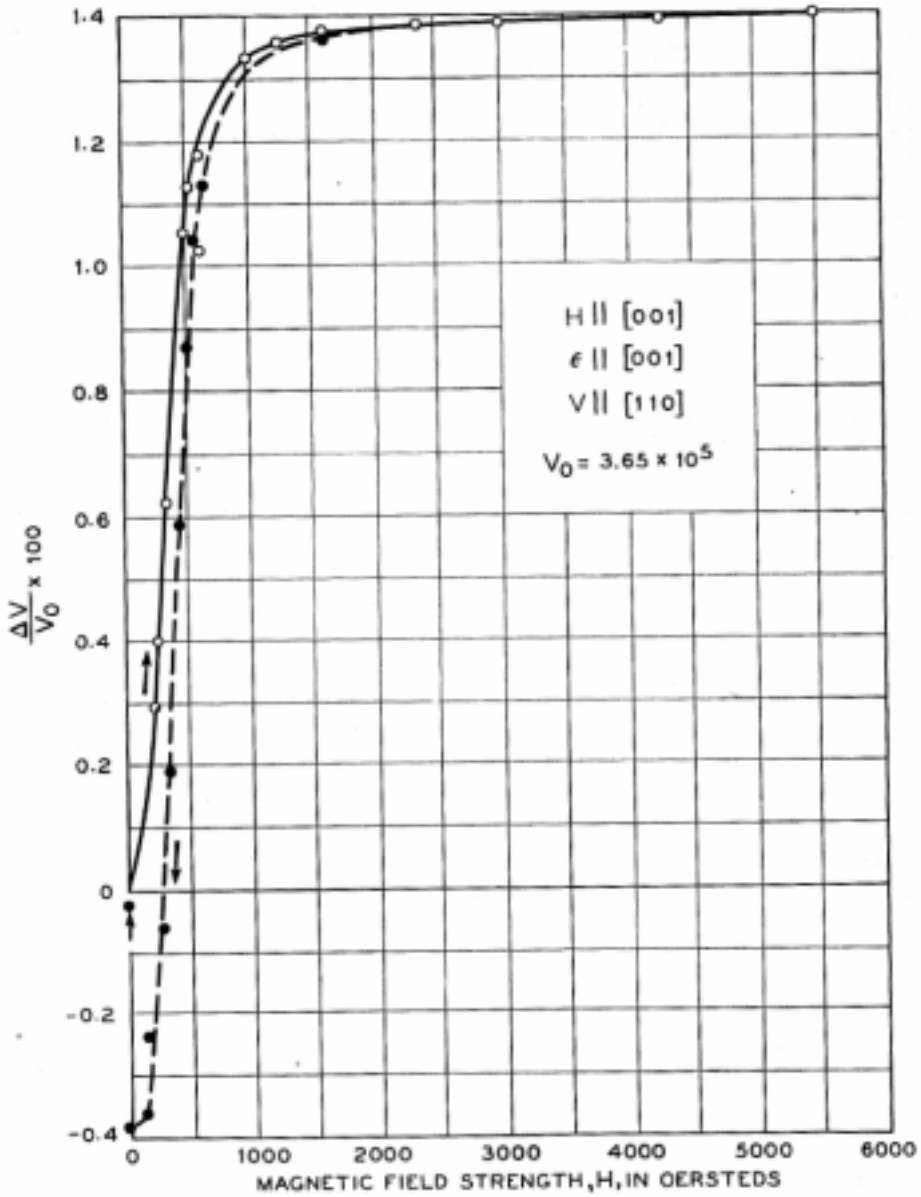

Fig. 5—Change in velocity in percent from demagnetized values as a function of the magnetizing field for a shear wave in a (110) section when the particle velocity is along the [001] direction and the field along the [001] direction.

Combining the elastic constants, the saturated elastic constants are evaluated:

$$c_{11}^s = 2.53, \qquad c_{12}^s = 1.58, \qquad c_{44}^s = 1.22, \quad (8)$$

all in 10^{12} dynes/cm^2.

It is obvious from the measurements of Figs. 4 to 8 that the changes in the elastic constants with magnetization are much smaller at the high frequencies (10 mc) than they are at the lower frequencies of 10 to 50 kilo-

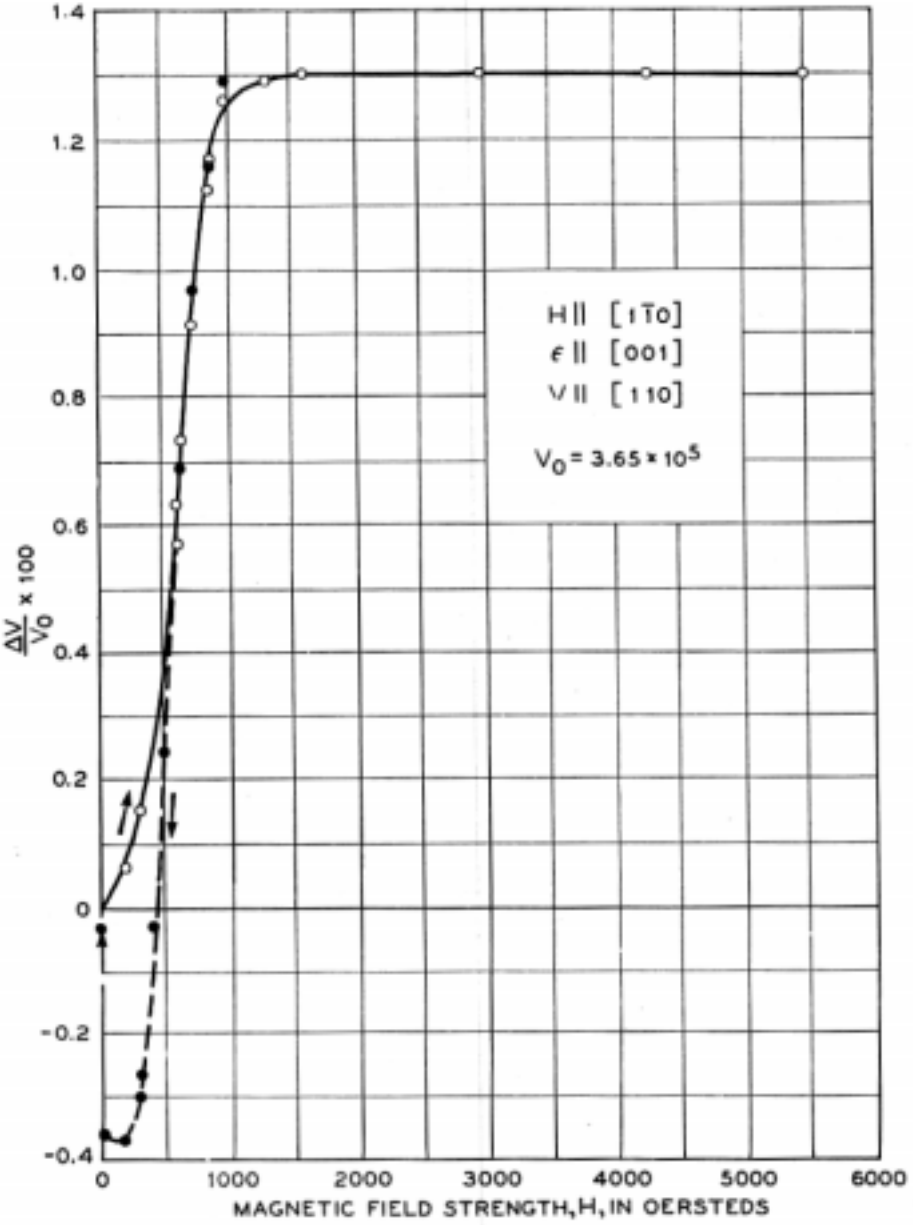

Fig. 6—Change in velocity in percent from demagnetized value as a function of the magnetizing field for a shear wave in a (110) section when the particle velocity is along the [001] direction and the field along the [1$\bar{1}$0] direction.

cycles where changes of 15 to 30 per cent have been observed in polycrystalline material.[3] A rough comparison of the low-frequency values with the 10 megacycle values can be obtained if we convert the observed changes in the c's to the equivalent change in E. This can be done if we use the method

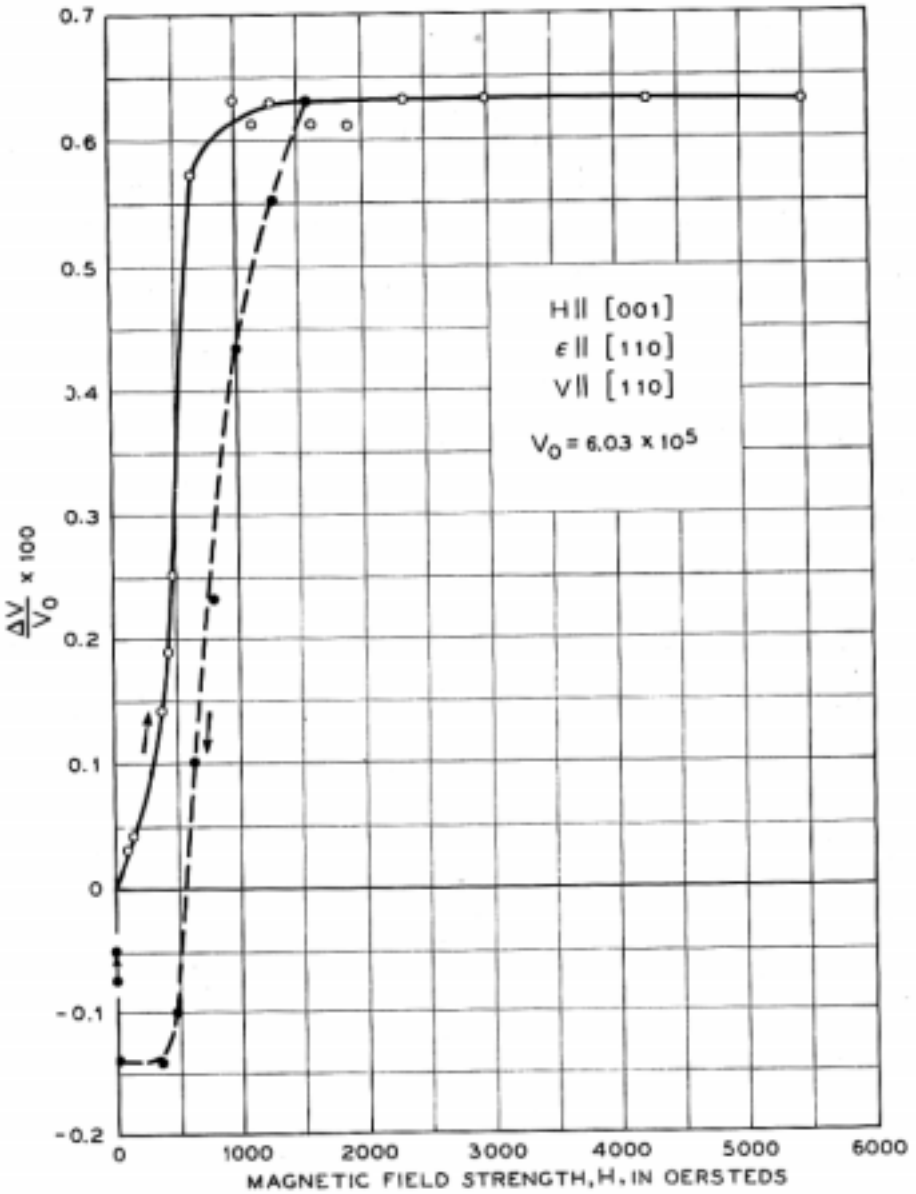

Fig. 7—Change in velocity in percent from demagnetized value as a function of the magnetizing field for a longitudinal wave in a (110) section when the particle velocity is along the [110] direction and the field along the [001] direction.

developed by one of the writers[9] for obtaining the elastic constants of a polycrystalline rod from the cubic elastic constants. In this case the Lamé elastic constants are given by the formulas

$$\lambda + 2\mu = \frac{3}{5}c_{11} + \frac{2}{5}c_{12} + \frac{4}{5}c_{44},$$
$$\mu = \frac{3}{5}c_{44} + \frac{c_{11} - c_{12}}{5}. \tag{9}$$

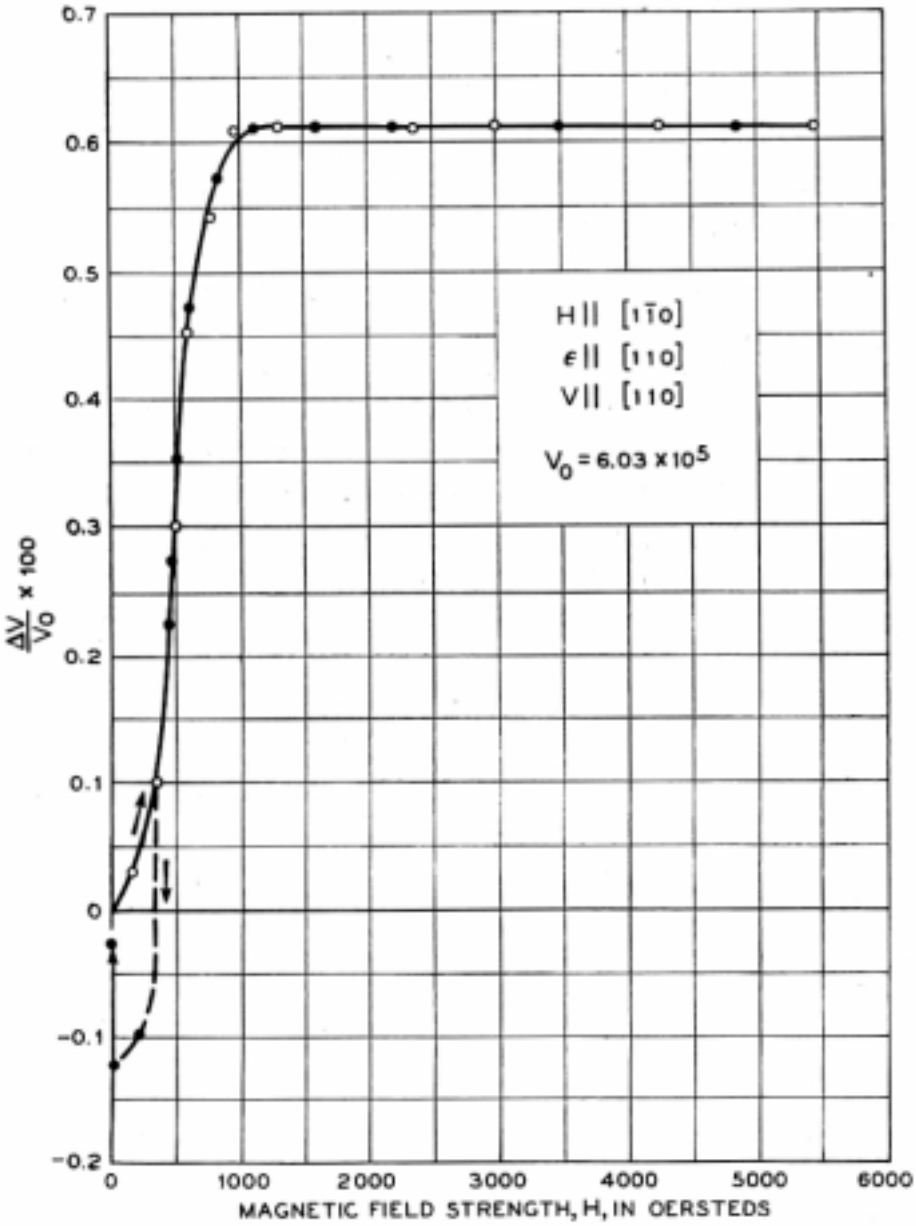

Fig. 8—Change in velocity in percent from demagnetized value as a function of the magnetizing field for a longitudinal wave in a (110) section when the particle velocity is along the [110] direction and the field along the [1$\bar{1}$0] direction.

Since in terms of the Lamé elastic constants, the value of Young's modulus is

$$E_0 = \mu\left(\frac{3\lambda + 2\mu}{\lambda + \mu}\right) \tag{10}$$

one finds that the difference between the saturated and demagnetized value of Young's modulus divided by the demagnetized value is

$$\frac{\Delta E}{E_0} = \frac{E_s - E_0}{E_0} = \frac{2.381 - 2.312}{2.312} = 0.03 = 3\% \qquad (11)$$

which is much smaller than that given by low frequency measurements.

To check our results, and be sure that the crystals were free from imperfections and strains, two other crystals were prepared and carefully annealed at 1100°C. The values found for the changes in elastic constants were considerably less for these crystals. The Q's of the crystal were also higher. Table II shows the measured values and the equivalent $\Delta E/E$ values. The table shows also the measurements for the demagnetized crystal of two Japanese workers[10,11] and the equivalent $\Delta E/E$ assuming that the saturated elastic constants are the same as those found for the other three crystals. Since these vary by only ± 0.5 per cent among themselves, this appears to be a good approximation.

TABLE II

ELASTIC CONSTANTS (IN 10^{12} DYNES/CM^2) AND ΔE-EFFECT IN SINGLE CRYSTALS OF NICKEL

Crystal	Magnetically Saturated			Demagnetized			$\Delta E/E$
	c_{11}	c_{12}	c_{44}	c_{11}	c_{12}	c_{44}	
1	2.53	1.58	1.22	2.50	1.60	1.185	0.03
2	2.524	1.538	1.23	2.52	1.54	1.229	0.0017
3	2.523	1.566	1.23	2.517	1.574	1.226	0.0046
Yamamoto[11]				2.44	1.58	1.02	0.16
Honda and Shirakawa[10]				2.52	1.51	1.04	0.11

The lower values of $\Delta E/E$ for the second and third crystals are probably due to larger domain sizes, caused by the longer anneal.

DAMPING AND ΔE-EFFECT IN POLYCRYSTALLINE RODS

To test the theory of micro-eddy-current shielding (see Introduction), the velocity and attenuation of elastic vibrations in well-annealed polycrystalline nickel rods were measured over the frequency range of 5 kilocycles to 150 kilocycles. In the method of measurement,[12] shown by Fig. 9, two matched piezoelectric crystals of resonance frequency corresponding to integral half wavelengths along the rod, are attached to the ends of the rod. Phase-amplitude balance was obtained by critical adjustment of frequency and output of the calibrated attenuator. The corresponding level was then compared with that obtained when the two crystals were cemented directly together. With little error, the velocity of propagation is given by

$$v = \frac{2fl_0}{n}, \qquad n = 1, 2, 3 \cdots \qquad (12)$$

The attenuation A (and hence the Q of the rod) was obtained by solving the equation

$$\sinh Al_0 = \frac{(r - \cosh Al_0)n\pi M_c}{Q_c M_R} \tag{13}$$

in which r is the ratio of output with crystals together to output with specimen attached, l_0 is the length of rod, M_c the mass of either crystal, M_R the mass of the rod, and Q_c the Q of the crystal as determined by resonance response method.

For this equation to apply accurately, the terminating impedance presented to the rod by the crystals at resonance must be small compared to the characteristic impedance of the rod, and the Q of the rod should be >10. This method may be used even when the total loss in the rod is so high that well defined resonances no longer exist. At the lower frequencies, however,

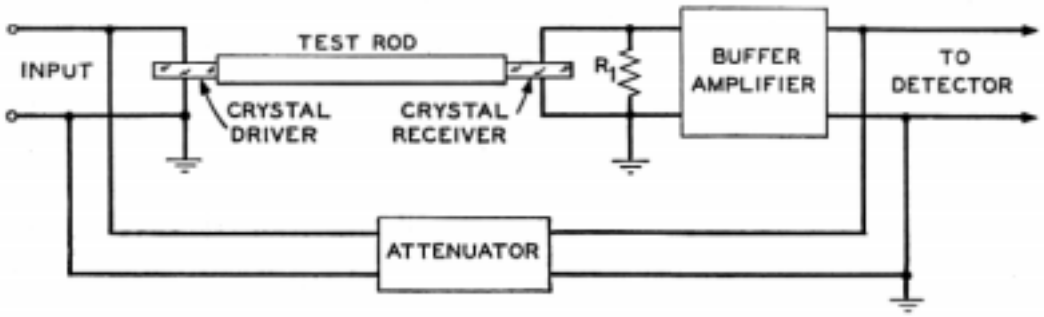

Fig. 9—Experimental arrangement for measuring the ΔE effect and associated loss in a polycrystalline rod at low frequencies.

a useful check may be made by the resonance response method of determining Q which involves determining the frequency separation Δf for two frequencies 3 db from the maximum response frequency, and using the formula

$$Q = \frac{f_{max}}{\Delta f} \tag{14}$$

Correction for the mass and dissipation of the piezoelectric crystals must of course be made. Both methods have been found to agree within about 10% —the probable error to be expected.

The Appendix lists formulae to be used when the resonance frequency of the crystal driver differs from the frequency at which phase balance is obtained. This condition of necessity occurred when the rods were subjected to a magnetic field, which caused an increase in the velocity of propagation.

Figure 10 shows a typical measurement of change in frequency and change in decrement with magnetizing field excited in a solenoid surround-

ing the nickel rod. Saturation is not quite obtained so that the ΔE effect measured is slightly lower than the true value, but for relative frequency comparisons this is not important.

The first rod measured was 0.320 cm in diameter and 10.16 cm long and was annealed at 1100°C. Five frequencies ranging from 22.5 kilocycles were

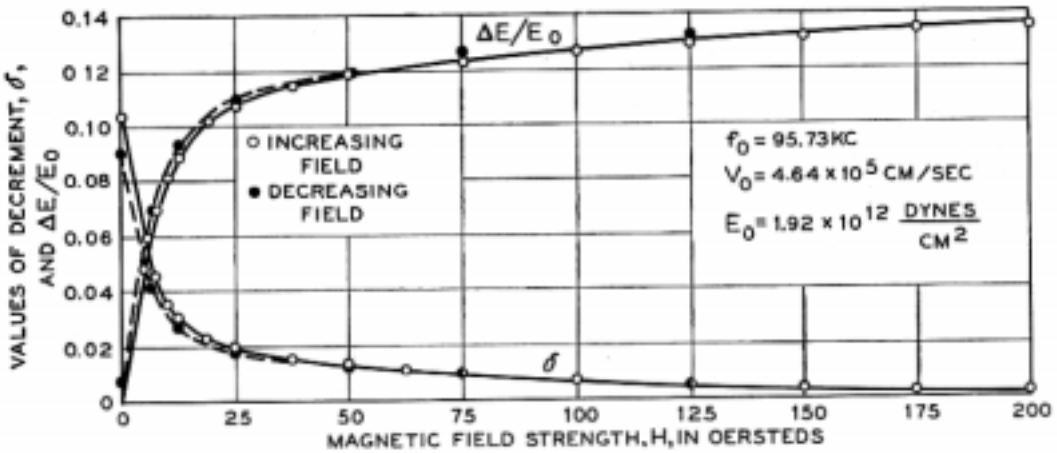

Fig. 10—Typical change in velocity and decrement of a polycrystalline rod as a function of the magnetizing field.

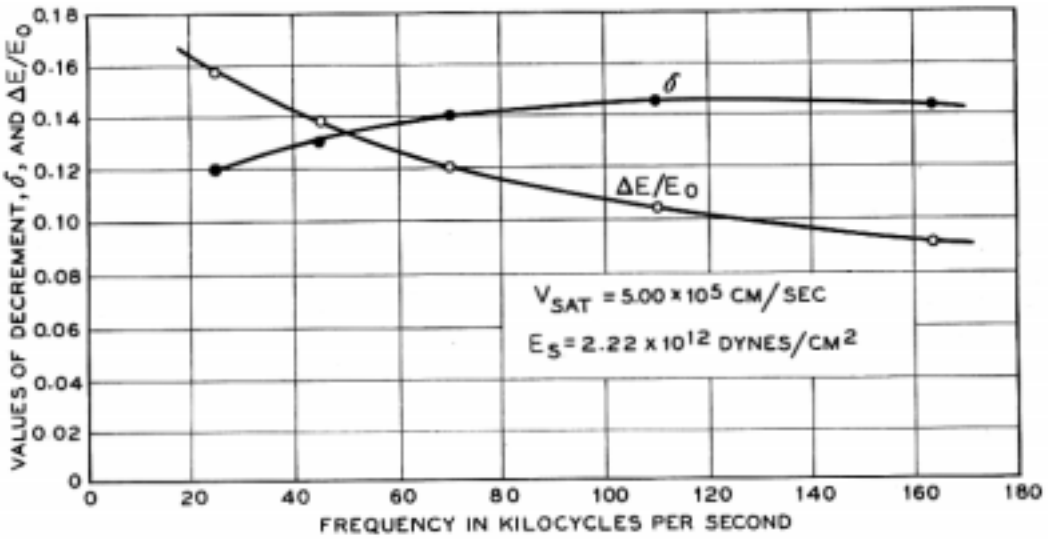

Fig. 11—Fractional change in Young's modulus, and the decrement, plotted as a function of frequency for rod No. 1.

used and the ratio of the change in Young's modulus to the value of Young's modulus for the demagnetized rod is shown plotted in Fig. 11. This figure shows also the decrement $\delta = \pi/Q$. It is obvious that the decrement eventually decreases as the frequency rises, and this is contrary to the simple theory of the micro-eddy-current effect,[3] which indicates that the decrement

should increase linearly with the frequency. The indicated maximum for this rod is below 120 kilocycles.

In order to obtain the first part of the decrement vs frequency curve, a rod of 46.05 cm length and 0.637 cm diameter was next used. This rod was annealed at 1050°C and presumably has a smaller average domain size than the first one, so that the important variations occur in a more favorable frequency range.

The changes in elastic constant and the decrement for this rod are shown by Fig. 12 for frequencies from 5 kilocycles to 96 kilocycles. At the lower frequencies the decrement increases in proportion to the frequency in

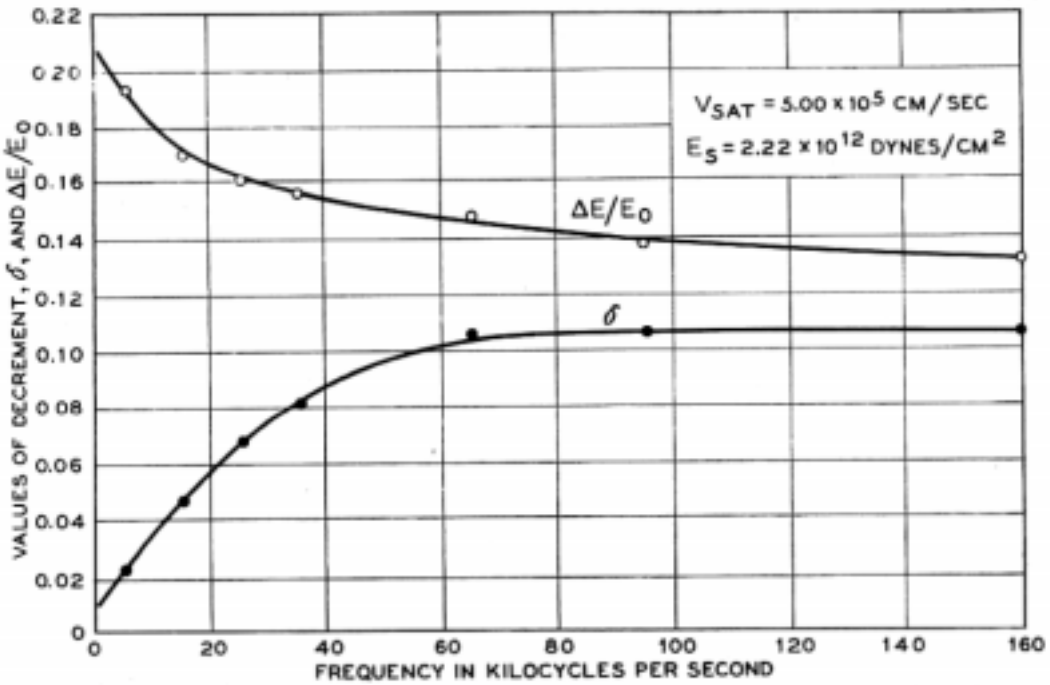

Fig. 12—Fractional change in Young's modulus, and the decrement, plotted as a function of frequency for rod No. 2.

agreement with the simple theory. By extending this curve down to zero frequency it is seen that a micro-hysteresis effect (which is independent of the frequency) gives an initial decrement of about 0.010. The decrement rises to an indicated maximum at somewhat more than 100 kilocycles and the change in elastic constant with saturation decreases with frequency.

The data on these two rods taken together indicate that there is a frequency of maximum decrement and for frequencies above and below this the decrement is smaller. The ΔE change in the elastic constant decreases as the frequency increases and for very high frequencies the ΔE effect becomes very small. As shown by the discussion in the next section, the fre-

quency of the maximum value of δ and the initial slope of the decrement frequency curve are connected with definite domain sizes which can be calculated approximately and compared with magnetic domain powder patterns.

Discussion

Our determinations of the *elastic constants* may be discussed in relation to the values obtained by others. The results reported by Honda and Shirakawa[10] and Yamamoto[11] were unknown to us and unavailable at the time of our preliminary communication. The data of the Japanese, converted from s-constants to c-constants by the relations:

$$c_{11} = \frac{s_{11} + s_{12}}{s_{11}^2 + s_{11}s_{12} - 2s_{12}^2}$$

$$c_{12} = \frac{-s_{12}}{s_{11}^2 + s_{11}s_{12} - 2s_{12}^2} \qquad (15)$$

$$c_{44} = 1/s_{44}$$

are included with our data in Table II.

As our experiments show, the 10 mc pulses that we used are so rapid that micro-eddy-currents largely prevent the stress-induced changes in magnetization from penetrating the domains. Therefore the constants determined by this method are those for material almost saturated. The values at saturation are independent of the initial domain distribution, and of the ease with which the magnetization in the separate domains can be changed by stress, consequently they are the more fundamental elastic constants of the material. The variety of values for unmagnetized nickel is made evident from the scatter in the ratios of $\Delta E/E$ that have been reported.[3] The variation in the values of the c-constants recently published is thus not surprising. The values at saturation of the three crystals examined by us are in substantial agreement, as shown in Table II. They cannot be compared directly with the results of the Japanese workers because the latter reported data for unmagnetized crystals only and then E is sensitive to heat treatment and domain configuration.

As mentioned in the introduction, the damping of elastic vibrations by micro-eddy-currents is proportional to the frequency at low frequencies (Eq. 1) and it rises with frequency to a maximum and then declines toward zero. The frequency at which the maximum occurs has been calculated[4] by using the equation of domain wall motion and evaluating the constants from the initial permeability and the power loss caused by domain wall motion. The maximum value of δ comes at the same value as that calculated

for eddy current losses in sheets having the same thickness as the domain, namely

$$l^2\mu_0 f_m/R = 0.13 \tag{16}$$

l being the thickness of the sheet, μ_0 the initial permeability, and R the resistivity of the material (all in c.g.s. units).

As noted below, the domain sizes calculated from the initial slope of the δ vs f curve of Fig. 12, and from the frequency at which the maximum decrement occurs, are respectively 0.035 mm and 0.045 mm (for plates). These values agree quite well. The decrement curve is broader than would be calculated from equation (1) for a single domain size. This agrees with the optical measurements of domain size by Williams,[6] which are shown by Fig. 13. This indicates domain sizes from 0.01 to 0.2 mm.

The maximum value for the decrement calculated from equation (1), using the measured values, is 0.35 compared to the observed value of 0.11. Part of this is due to the broadening of the peak caused by a distribution of domain sizes, but part may also be due to the deviation of the actual domain shape from a sheet which has been assumed in making the calculations.

The calculations of domain size are made in more detail as follows:

According to Döring[13] the change in Young's modulus for nickel containing only small internal strains is related to the initial permeability, μ_0, as follows:

$$\frac{\Delta E}{E_0} = -\frac{\lambda_{111}^2(\mu_0 - 1)E_s}{5\pi I_s^2}\left[\frac{5c_{44}}{c_{11} - c_{12} + 3c_{44}}\right]^2 \tag{18}$$

provided the averaging over all crystallites is carried out with constant strain. (If constant stress is assumed, the fraction in brackets, equal to 1.76, is omitted.) For nickel λ_{111} is 25×10^{-6}, I_s is 484, and the c's are the elastic constants given in Table I. This equation holds for low frequencies at which the shielding in single domains is negligibly small. When the relaxation effect of domain wall motion is considered[4] equation (18) has to be multiplied by the factor

$$1/(1 + f^2/f_0^2) \tag{19}$$

The data of Fig. 12 give the values:

$$E_0 = 1.83 \times 10^{12}, \qquad E_s = 2.22 \times 10^{12}\ \text{dynes/cm}^2, \frac{\Delta E}{E} = 0.21 \tag{20}$$

for low frequencies. Using these in the above equation, the calculated value of μ_0 is 320. A direct measurement* of μ_0 has been made for this rod and found to be 340, in good agreement with that deduced from the ΔE effect.

* Measurements were made independently by Miss M. Goertz and Mr. P. P. Cioffi in order to check this unusually high value.

Since the permeability is much higher than can be accounted for by domain rotation it is obvious that domain boundary motion is occurring. Hence in determining the domain sizes from the slope of the decrement vs

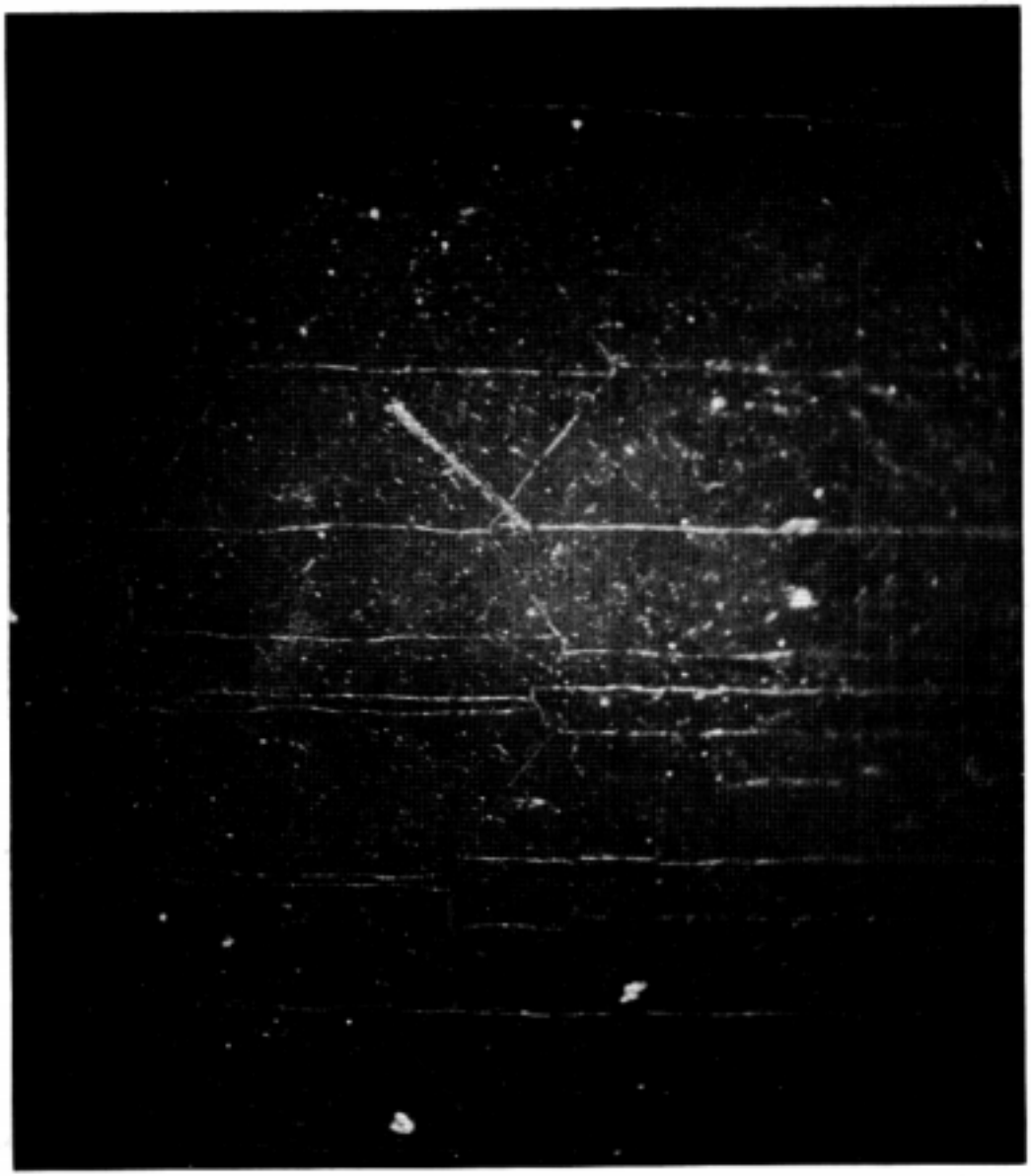

Fig. 13—Photograph of domains in a single nickel crystal (after Williams). Field of view, 0.5 mm.

frequency curve, equations (1) and (2) for domain boundary motion are appropriate.

When the data of Fig. 12 are extrapolated to zero frequency it appears that there is a microhysteresis loss (which is independent of the frequency) giving a decrement of 0.01. The initial slope of the δ_i vs f curve is then about